SCCC Turbo Equalizer/Decoder for X-band Nano Satellite High-Speed Downlink System

By Naohiko IWAKIRI[1)], Hirobumi SAITO[2)], and Shinichi NAKASUKA[1)]

[1)]*Department of Aeronautics and Astronautics, The University of Tokyo, Tokyo, Japan*
[2)]*The Institute of Space and Astronautical Science, Sagamihara, Japan*

Nano satellite technologies have been recognized as potential candidates for new satellite applications. We have developed a X-band downlink system for nano satellite employing Consultative Committee for Space Data Systems (CCSDS) 131.2-B-1 signaling formats with a modulation symbol rate of 100 Msps. Since nano satellites with a mass of less than 50 kg have more constraints than typical large satellites, the received signals of nano satellites tend to suffer much more distortion due to the system and channel constraints. To compensate for the distortion, several techniques have been developed to provide higher data rate than 100 Mbps for nano satellites. At the transmitter, a look-up table (LUT) based digital predistorter for memoryless AM/AM and AM/PM nonlinearities is designed to mitigate nonlinearity of power amplifier (PA) and IQ-imbalance of quadrature modulator. At receiver side, a soft interference canceller (SIC) turbo equalization combined with SCCC turbo decoder has developed to overcome nonlinear/linear distortion using iterative techniques. For 16-QAM modulation, a nonlinear compensation technique based on centroid estimation at the receiver is also developed to correct constellation points of received signals. The techniques are modeled and verified via computer simulation; therefore, the obtained results apply to the downlink system designs of the nano satellite, "Hodoyoshi 4".

Key Words: GaN PA, Nano satellite communication system, Predistortion, Turbo code, Turbo equalizer

1. Introduction

Japan's nano-satellite center (NSC) is developing new nano-satellite technology to realize new industrial space systems and services [1)]. Several nano satellites have been developed and launched in resent years [2)]. Different applications as well as scientific missions have been proposed for future satellite industry [3)]. A high-speed downlink system specialized to nano satellites is consequently required to achieve the various missions. However, since conventional high-speed downlink systems have been designed for large satellites, constraints for the transmitter of nano satellite with a mass of less than 50 kg are more severe than those for large satellites due to low-power, lightweight, and low-cost modules. Thus, high-speed downlink system specialized to nano satellites must be developed for future satellite applications.

Consultative Committee for Space Data Systems (CCSDS) 131.2-B-1 recommendation [4)] published to support a wide range of spectral efficiency values and data rates for high-data-rate telemetry applications in March 2012. Comprehensive coding and modulation schemes are defined as adaptive coding and modulation (ACM) formats including serially concatenated convolutional turbo coding (SCCC) with various data rate using punctured code and *m*-ary modulation, where the modulation efficiency *m* is set to 4, 8, 16, 32, and 64. The system design and evaluation can be found in the literature [5-8)]. The downlink systems employing this standard for large satellites with the data rate more than 1 Gbps have been reported [5, 6)].

The characteristics of a satellite channel are nonlinear and dispersive owing to both amplitude and phase distortion. Moreover, a high-speed satellite communication system is likely to degrade performances owing to channel- or circuit-induced factors.

To achieve high-speed transmission and overcome the above difficulties, we have developed a X-band downlink system for nano satellites employing the CCSDS 131.2-B-1 signaling formats of m = 4 and 16 with a modulation symbol rate of 100 Msps. At the receiver, SCCC turbo decoder combined with a soft interference canceller (SIC) turbo equalizer and distortion compensation techniques has been developed to obtain the maximum possible coding gain for each ACM format [9)]. At the transmitter, a look-up table (LUT) based digital predistorter (DPD) for memoryless nonlinear channels has been designed to mitigate nonlinearity of power amplifier (PA) and IQ-imbalance of quadrature modulator [10)]. The linear/nonlinear distortion sources based on experimental measurements were modeled, and then the downlink system performances were evaluated via simulation using a signal processing worksystem (SPW) [11)]. The results indicate data rate beyond 100 Mbps [9, 10)].

Since several newly developed modules on the transmitter engineering model (EM) have been implemented, the more accurate degradation factors can be modeled based on the measurements. Specifically, the 2 W GaN-based high PA (HPA) of class AB have developed for the nano satellite transmitter, and then a practical PA model is also designed to approach more accurately reflect the actual output waveform of the transmitter EM. The system simulation combined with the modified PA model is expected to obtain a more accurate performance than previous works.

This paper is organized as follows. The downlink system structure are summarized in Section 2. The practical PA modeling are described in Section 3. The system performance

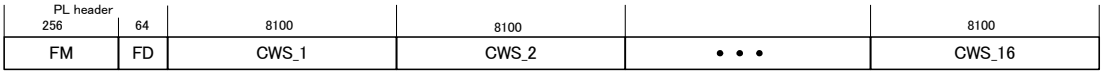

Fig. 1. Physical layer frame structure of CCSDS 131.2 B-1.

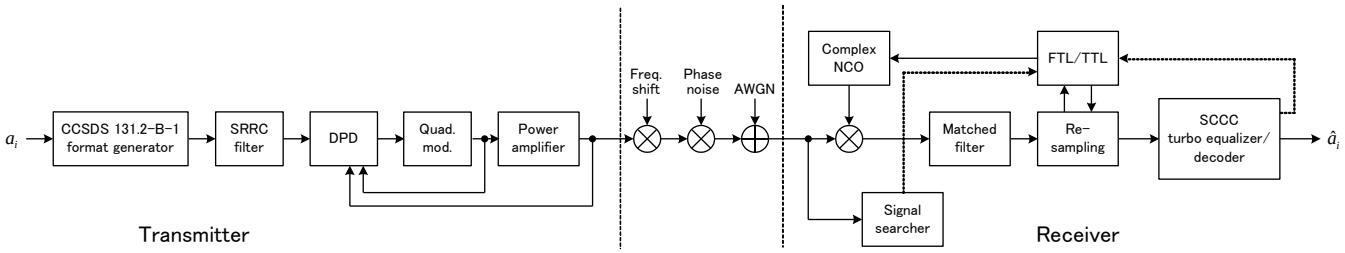

Fig. 2. System block diagram.

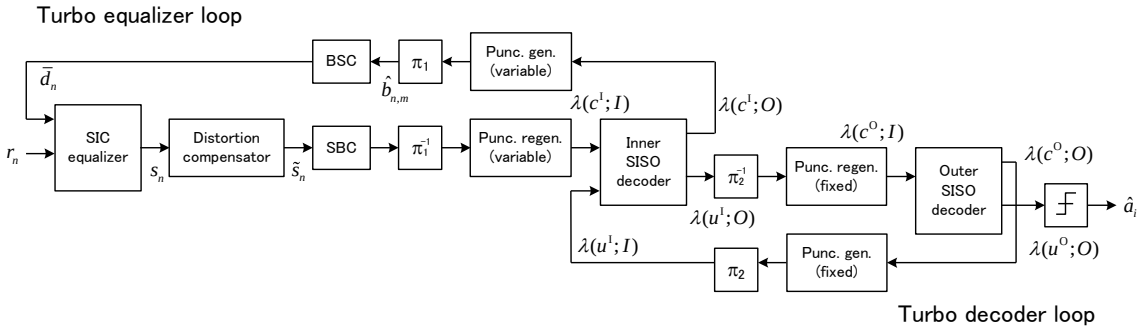

Fig. 3. Block diagram of SCCC turbo equalizer/decoder.

analyses via computer simulation are discussed in Section 4. Finally, conclusions are given and future work is outlined in Section 5.

2. Downlink System Structure

2.1. Signaling Format

In CCSDS 131.2-B-1 recommendation, a physical layer (PL) frame consists of a PL header followed by 16 codeword sections (CWSs), as shown in Fig. 1. The PL header is composed of a frame maker (FM) of 256 known symbols for the initial acquisition, and a frame descriptor (FD) of 64 encoded symbols with mapping 16 information bits of the ACS format number to a 64 bit code word. Since each CWS consists of 8100 modulation symbols regardless of the selected ACM format, common modules can be implemented after the packet generator because the modulation symbols have a fixed symbol rate regardless of the ACM format. After calculating link budget for the planned nano satellite downlink, the capacity limits dictated ACM formats 1 to 6 and 13 to 17 that can be transmitted over the nano satellite channel. In other words, the possible modulation efficiencies are m of 4 and 16. The relationship between the number of information bits and coding rates per CWS is listed in Table 1. Note that 16-QAM is adopted instead of 16-APSK for m = 16 since the minimum

Table 1. ACM formats of high-speed downlink system.

QPSK			16-QAM		
ACM	Info. bits	Rate	ACM	Info.bits	Rate
1	5758	0.355	13	19198	0.593
2	6958	0.430	14	21358	0.659
3	8398	0.518	15	23518	0.726
4	9838	0.607	16	25918	0.800
5	11278	0.696	17	28286	0.874
6	13198	0.815	8100 mod. symbols per CWS		

Table 2 System specification.

RF center frequency	8160 MHz
HPA output	2 W
SRRC filter	α = 0.5, 64 taps
Mod. symbol rate	100 Msps
Oversampling frequency	400 MHz
SCCC encoder	Generator polynomials (octal): 7, 5, r = 1/2, 4-state RSC code
MAP-Decoder	BCJR algorithm Number of iterations = 16
Equalizer	$P(f)$: LF = 13 taps, fractional 1/2 $Q(f)$: LB = 7 taps, fractional 1
Adaptive algorithm	LMS (μ = 0.015/0.005),

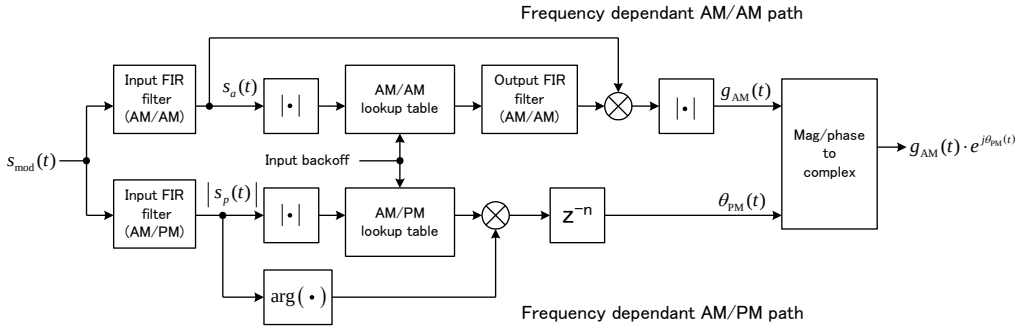

Fig. 4. Block diagram of PSB model.

Euclidean distance between constellation points of the former is larger than that of the latter and the effective compensation techniques against linear/nonlinear distortion have been developed. However, 16-APSK modulation is also implemented in the experimental system to carry messages according to CCSDS 131.2-B-1 recommendation and compare the performance of the 16-APSK system with that of the 16-QAM in the nano satellite channel.

2.2. System Structure

A block diagram of the equivalent lowpass model [12] for the nano satellite high-speed downlink system is shown in Fig. 2. These blocks except the power amplifier have the same features as the previous work [9, 10]. The system specifications used in evaluations are listed in Table 2.

On the transmitter side, a CCSDS 131.2-B-1 format generator outputs modulation symbols that consist of in-phase and quadrature (IQ) components, depending on the selected ACM format, and then the modulation symbols are passed to a square-root raised cosine (SRRC) filter followed by DPD, quadrature modulator, and PA.

On the receiver side, a downconverted complex baseband signal with an oversampling factor of 4 is input into the receiver, as shown in Fig. 2. This input is first processed by a signal searcher to obtain the PL header timing by correlating the received signals with the known FM symbol sequence. After finding the timing with the maximum correlator output, the initial parameters, such as frequency deviation, phase offset, and tap weights of SIC equalizer, are estimated, and then these parameters are passed to frequency tracking loop (FTL), time tracking loop (TTL), and SIC equalizer, respectively. The FTL removes the residual Doppler frequency and carrier phase offset from the input signals based on the Costas loop [12]. On the other hand, the TTL provides the optimum symbol timing based on the Gardner loop [12], and then sends the suitable symbols (operating at twice the modulation symbol rate) to the SCCC turbo equalizer/decoder as shown in Fig. 3. The two feedback loops operate according to turbo principle [13]. Specifically, the upper feedback loop, SIC turbo equalizer, adaptively compensates linear/nonlinear distortion when updating tap weights of forward and backward FIR filters to minimize the errors between the received symbol and iteratively reproduced symbol. The lower loop, SCCC turbo decoder, decodes the code sequences in an iterative fashion, and thus outputs the hard-decision bit sequence and the soft-decision modulation symbol sequence. More details of the SCCC turbo equalizer/decoder can be found in the previous paper [9].

3. PA Modeling

3.1. PSB Model

Different PA modeling techniques have been proposed in the literature [11, 14, 15]. There are two main categories of PA models: analytical model and empirically based model. Since we have obtained measurements of the different HPAs and want to evaluate system performances using the equivalent lowpass model with reasonable complexity, the empirical model, called Poza-Sarkozy-Berger (PSB) model [12], has been selected and implemented as the PA model shown in Fig. 2. The PSB model consists of two branches as shown in Fig. 4. The upper branch, including a LUT, and pre- and post-filters, is configured to model an AM/AM path and output distorted gain $g_{AM}(t)$. The measured AM/AM and AM/PM characteristics at the center frequency are stored in the LUT to generate memoryless distortion. The pre- and post-filters yield frequency dependence corresponding to finite impulse response (FIR) filter whose tap weights are obtained by finding horizontal and vertical shift values from the AM/AM curve of the reference center frequency. Similarly, the lower branch is configured to model AM/PM path and output distorted phase $\theta_{PM}(t)$. Finally, the gain and the phase are transformed into complex signals.

3.2. Two Stage PA model

Recently, GaN high electron mobility transistors (HEMTs) are promising PA devices to improve power added efficiency (PAE) for wireless communications. Then, we develop GaN HPA of class AB achieved more than 40 percent PAE of and the bandwidth of 200 MHz in X-band.

The performances required for PSB model were measured. In Figure 5, the AM/AM curve is almost linear below the output power of 34 dBm, whereas the output power gradually saturates with input power and has no saturation level within

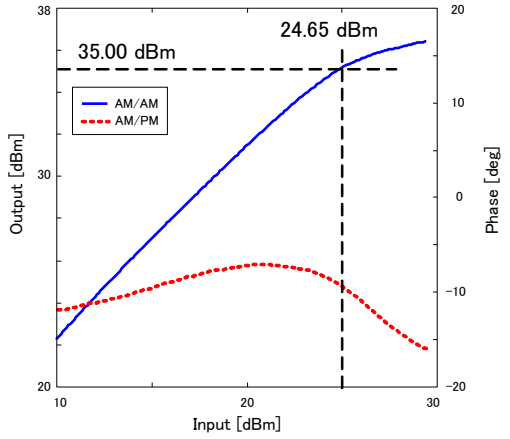

Fig. 5. Performances of GaN HPA at reference frequency.

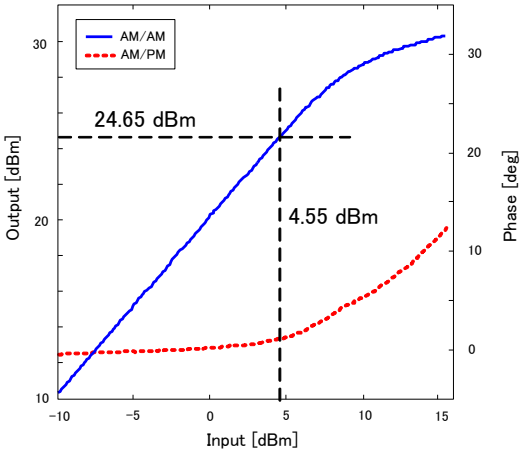

Fig. 7. Performances of driver amplifier at reference frequency.

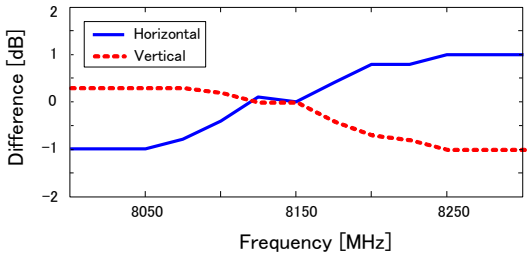

(a) AM/AM portion

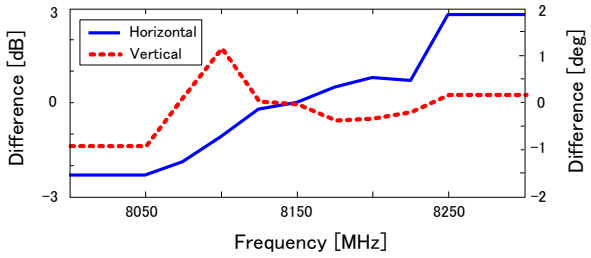

(b) AM/PM portion

Fig. 6. Horizontal and vertical shift differences of GaN HPA.

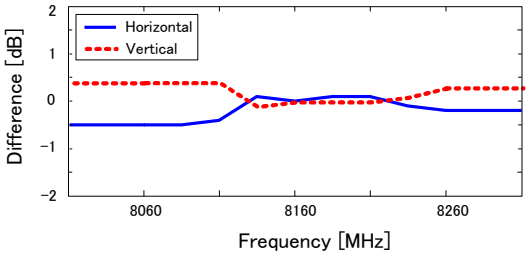

(a) AM/AM portion

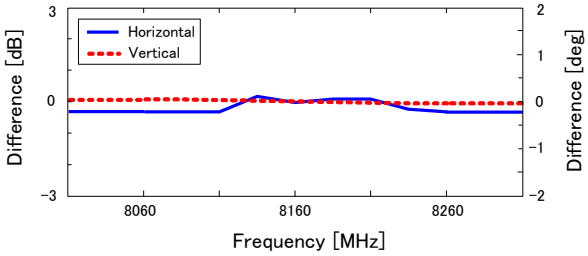

(b) AM/PM portion

Fig. 8. Horizontal and vertical shift differences of driver amplifier.

the practical input power range. The AM/PM curve varies by only several degree. The frequency dependence of AM/AM and AM/PM characteristics are plotted in Figs. 6 (a) and (b), respectively. The proper values of horizontal and vertical displacements are found using MMSE estimation given by the shift values between the characteristic curves of the reference frequency and all other frequencies. Since target symbol rate is 100 Msps in X-band, the measurements at 9 frequencies from 8100 to 8300 MHz with 25 MHz steps are chosen for the PSB model. In Fig. 6 (a) horizontal and vertical shift values corresponding to input and output powers of the AM/AM curve are within 2 dB. In Fig. 6 (b), the horizontal shift value of AM/PM ranges about 5 dB, and the vertical shift value indicating phase differences ranges about 3 degree.

The PA module implementing on the transmitter EM is constructed from two amplifiers, a driver amplifier followed

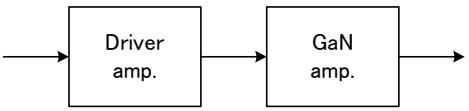

Fig. 9. 2 stage PSB model.

by the GaN HPA. To obtain the modeling output signal closer to the EM output, we design a two stage PSB model using two kinds of amplifier measurements, as shown in Figs. 5 - 8. The AM/AM and AM/PM curves of driver amplifier indicate that the output signal will suffer much less from nonlinear distortion when setting the operating point below the input power of 5 dBm, as shown in Fig. 7. Below, we give the procedure for implementing the two PSB model with respect

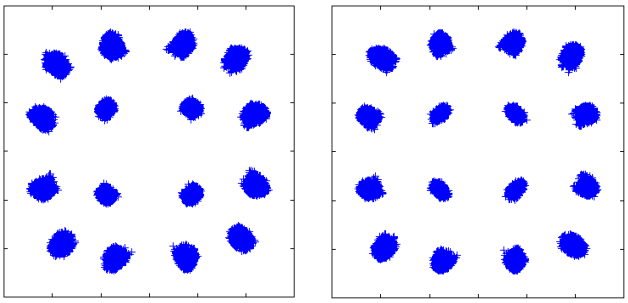

(a) Without DPD (b) With DPD

Fig. 10. Scatter plots for 16-QAM received signal distorted by a combination of two stage PSB model.

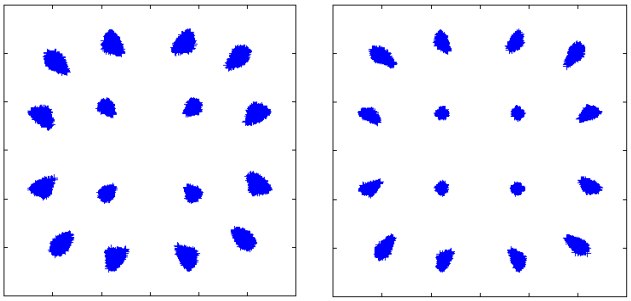

(a) Without DPD (b) With DPD

Fig. 11. Scatter plots for 16-QAM received signal distorted by a combination of memoryless PA model.

to the block diagram of two stage PSB model, as shown in Fig. 9. As indicated by the vertical dotted line in Fig. 7, the operating point of input power of the driver amplifier is set to 4.55 dBm to avoid the nonlinear region, and then the output power of 24.65 dBm is obtained. This power is assigned to the input power of the GaN HPA, as indicated by the vertical dotted line in Fig. 5. Therefore, the output power of 35 dBm corresponding to the input power of 24.65 dBm is obtained. Since the actual output power of the transmitter EM includes the power loss of circuits and cables, the system loss is assumed to be 2 dB for the simulation model. Note that the operating point is defined as the average power of the input signal to each amplifier.

3.3. Comparison of Scatter Plot

The effects of distortion caused by different PA models at the sampling instant are readily seen in scatter plots for received 16-QAM signals. The scatter plots with or without DPD for the two stage PSB model are illustrated in Fig. 10. For comparison, the scatter plots for memoryless two stage PA model are also illustrated in Fig. 11. This model uses only the two LUTs as shown in Figs. 5 and 8. The effects of two PA models can be seen in the scatter plots in Figs. 10 (a) and 11 (a). As expected, each constellation point of the two stage PSB model indicates smaller distribution than that of the memoryless model. In other words, the PA model with memory causes severe intersymbol interference (ISI). Comparing with or without DPD for the two stage PSB model,

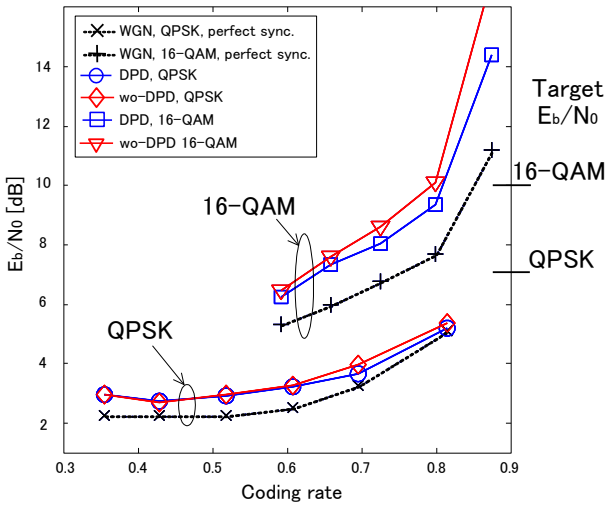

Fig. 12. Required E_b/N_0 for BER = 10^{-6} on two stage PSB model with or without DPD.

the dispersion of each of the predistorted constellation points has smaller than that of non-predistortion. The shape of the predistorted constellation is improved around vertexes and closes to the original square constellation points, as shown in Fig. 10. However, since the DPD is unable to reduce the ISI sufficiently, the residual ISI must be eliminated by using the SCCC turbo equalizer/decoder at the receiver.

4. Performance Evaluation of Downlink System

The nonlinear distortion caused by the PA has a significant impact on performance loss. The received signals are also affected by other channel impairments, and then the impairments, such as IQ imbalance, frequency shift, phase noise, and WGN, are modeled as shown in Fig. 2. We assume that the parameters are set to IQ imbalance of 5 degree, frequency shift of 1 kHz, and the phase noise mask corresponding to X-band signal [16]. To evaluate the downlink system performances, the values of E_b/N_0 required to achieve a BER of 10^{-6} for all ACM formats with or without the DPD are simulated, as shown in Fig. 12. The curves corresponding to perfect synchronization are also shown as dotted lines. Note that the horizontal axis represents coding rate corresponding to each ACM format as listed in Table 1. Comparing with or without the DPD, the differences between the required E_b/N_0 curves are almost the same for QPSK modulation. On the other hand, for 16-QAM modulation, the required E_b/N_0 curves of with the DPD become less steep, leading to more of E_b/N_0 difference as the coding rate increases. Since ACM formats of 16-QAM with higher coding rate are more susceptible to channel impairments owing to the lower coding gain, the residual ISI and phase variation seriously degrades BER performance, especially of without the DPD.

The link budget for nano satellite downlink was found by setting transmit power of 2 W. The obtained target E_b/N_0 for QPSK and 16-QAM are 7 dB and 10 dB, respectively. The simulation results imply that all ACM formats of QPSK

modulation with or without DPD are acceptable for the target E_b/N_0; the required coding rates of ACM formats of 16-QAM for with or without DPD are 0.80 and 0.726, respectively. Assuming modulation symbol rate of 100 Msps in the nano satellite downlink channel, the 16-QAM system with DPD of ACM 16 will achieve the data rate up to 320 Mbps, whereas the QPSK system will achieve the data rate up to 162 Mbps.

5. Conclusions

This paper has presented performance evaluation of X-band nano satellite high-speed downlink system with symbol rate of 100 Msps in practical nano satellite channel. Since general modules with a small, lightweight, and low-power are required for the onboard transmitter, the resulting transmitted signals suffer from greater linear/nonlinear distortion than those of a custom-designed satellite transmitter; consequently, effective compensation techniques for nano satellite high-speed downlink system are required. We have developed a SCCC turbo decoder combined with a SIC turbo equalizer and distortion compensation techniques at the receiver, and a LUT based DPD at the transmitter. The system performances are evaluated by modeling linear/nonlinear distortion sources based on experimental measurements to obtain the modeling output signal closer to the transmitter EM output. The simulation results indicate that the maximum data rate of 320 Mbps for 16-QAM and 162 Mbps for QPSK are achieved.

We have been developing a downlink system for NSC nano satellites, "Hodoyoshi 4". Since different challenging tasks must be solved to complete the downlink system, the simulation results support the system implementation point of view, such as to obtain suitable LUT tables adapting temperature variation at the transmitter and design digital circuit on FPGA at the receiver. The completed transmitter and receiver will be verified by using the nano satellite, "Hodoyoshi 4", and then provide high-speed downlink communications beyond 100 Mbps for nano satellite.

Acknowledgments

This research is granted by the Japan Society for the Promotion of Science (JSPS) through the "Funding Program for World-Leading Innovative R&D on Science and Technology (FIRST Program)," initiated by the Council for Science and Technology Policy (CSTP).

References

1) http://park.itc.u-tokyo.ac.jp/nsat/main.html
2) H. Saito: Small satellite REIMEI for aurora observation -five years orbit-, *Proc. International Conference on Space, Aeronautical and Navigational Electronics 2010* (*ICSANE 2010*), SANE 2010-96.
3) S. Nakasuka: From Education to Practical Use of Nano-satellites - Japanese University Challenge towards Low Cost Space Utilization -, *Proc. 8th IAA Symposium on Small Satellite for Earth Observation*, Apr. 2011.
4) CCSDS 131.2-B-1: Flexible advanced coding and modulation scheme for high rate telemetry applications, *ESA, draft blue book*, Mar. 2012.
5) K. S. Andrews, A. Argueta, N. E. Lay, M. Lyubarev, E. H. Sigman, M. Srinivasan, and A. Tkacenko: Reconfigurable wideband ground receiver hardware description and laboratory performance," *Interplanetary Network Progress Report*, vol. 42-180, Feb. 2010, pp. 1-22.
6) S. Benedetto, R. Garello, and G. Montorsi: MHOMS, high-speed ACM modem for satellite applications, *IEEE Wireless Commun*., Apr. 2005, pp. 66-76.
7) G. P. Calzolari, E. Vassallo, New coding and modulation schemes for future CCSDS missions, *TTC 2010*, Sep. 2010.
8) M. Bertinelli, P. Burzigotti, G. Montorsi, and E. Vassallo, ESA advanced coding and modulation performance under realistic channel conditions, *CCSDS SLS-RFM & SLS-CS WG meeting*, Oct. 2009, SLS-RFM_09-09.
9) N. Iwakiri, A. Tomiki, T. Mizuno, H. Saito, and S. Nakasuka: Performance analysis of SCCC turbo equalization with nonlinear satellite channel compensation techniques for nano/small satellite high-speed communication systems, *Proc. International Conference on Space, Aeronautical and Navigational Electronics 2011* (*ICSANE 2011*), Oct. 2011, SANE-66.
10) N. Iwakiri, H. Saito, and S. Nakasuka: Turbo equalizer/decoder performances of nonlinear channels due to different classes of GaN HPAs for X-band nano satellite high-speed downlink system," *Proc. International Conference on Space, Aero- nautical and Navigational Electronics 2012* (*ICSANE 2012*), Oct. 2012, SANE-71.
11) http://www.synopsys.com/systems/blockdesign/digitalsignalprocessing/pages/signal-processing.aspx
12) M. C. Jerichim, P. Balaban, and K. S. Shanmugan: *Simulation of Communication Systems, 2nd ed*., Kluwer Academic/Plenum Press, New York, 2000.
13) J. Hagenauer: The turbo principle: Tutorial introduction and state of the art, *Proc. Int. Symp. on Turbo Codes*, Sep. 1997, pp. 1–11.
14) A. Tkacenko: Wideband power amplifier modeling incorporating carrier frequency dependent AM/AM and AM/PM characteristics, *Interplanetary Network Progress Report*, vol. 42-180, Feb. 2010, pp. 1-34.
15) F. M. Ghannouchi and O. Hammi: Behavioral modeling and predistortion, *IEEE Microw. Magazine*, vol. 2, no. 4, Dec. 2009, pp. 52-64.
16) M. Bertinelli, P. Burzigotti, G. Montorsi, and E. Vassallo: ESA advanced coding and modulation performance under realistic channel conditions, *CCSDS SLS-RFM & SLS-CS WG meeting*, Oct. 2009, SLS-RFM_09-09.